Influences of Geometric Configurations of Bypass Grafts on Hemodynamics in End-to-Side Anastomosis

Jae-Sung Choi, M.D., Ph.D.*, Sung Chul Hong**, Hyuck Moon Kwon, M.D., Ph.D.***,
Sang-Ho Suh, Ph.D.****, Jeong Sang Lee, M.D., Ph.D.*

Background: Although considerable efforts have been made to improve the graft patency in coronary artery bypass surgery, the role of biomechanical factors remains underrecognized. The aim of this study is to investigate the influences of geometric configurations of the bypass graft on hemodynamic characteristics in relation to anastomosis. ***Materials and Methods:*** The Numerical analysis focuses on understanding the flow patterns for different values of inlet and distal diameters and graft angles. The Blood flow field is treated as a two-dimensional incompressible laminar flow. A finite volume method is adopted for discretization of the governing equations. The Carreau model is employed as a constitutive equation for blood. In an attempt to obtain the optimal aorto-coronary bypass conditions, the blood flow characteristics are analyzed using *in vitro* models of the end-to-side anastomotic angles of 45°, 60° and 90°. To find the optimal graft configurations, the mass flow rates at the outlets of the four models are compared quantitatively. ***Results:*** This study finds that Model 3, whose bypass diameter is the same as the inlet diameter of the stenosed coronary artery, delivers the largest amount of blood and the least pressure drop along the arteries. ***Conclusion:*** Biomechanical factors are speculated to contribute to the graft patency in coronary artery bypass grafting.

Key words: 1. Coronary artery bypass
2. Computer simulation
3. Anastomosis, surgery
4. Hemodynamics

INTRODUCTION

A great deal of effort has been put into avoiding bypass graft failure and improving graft patency in coronary artery bypass surgery, including through the use of arterial graft instead of saphenous vein. However, the role of biomechanical factors, which could initiate progress of focal intimal hyperplasia around the anastomosis and finally cause graft failure, has been relatively little known [1-4]. For the initiation and development of atherosclerosis in the arteries, four hemodynamic hypotheses have been postulated, namely, the pressure-related hypothesis [5], high wall shear stress hypothesis
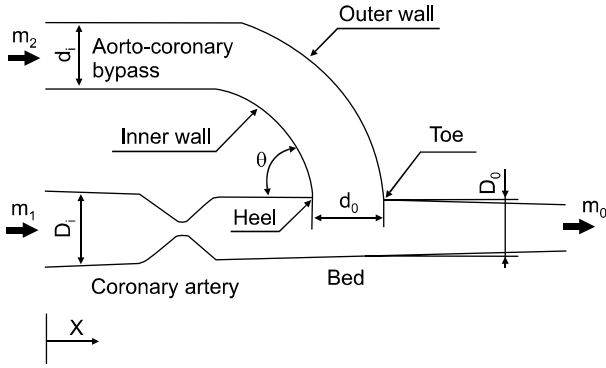
Fig. 1. Geometric configuration of end-to-side coronary artery bypass grafting (m=Mass flow rate; d=Diameter of bypass graft; D=Diameter of coronary artery).

[6], low wall shear stress hypothesis [7], and turbulence-related hypothesis [8]. However, the pathogenesis of the initiation and progression of the disease is not yet completely understood.

Biomechanical factors are related to fluid dynamics or wall mechanics. Low-wall shear stress and high-wall mechanical stress/strain are the primary biomechanical factors predisposing a patient to coronary bypass graft disease [9]. Various factors including vessel geometry and coronary artery movement have been identified as directly affecting the primary biomechanical factors [10-12]. Several authors [13,14] have reported the results of some numerical analysis for the flows in end-to-side anastomosis.

The aim of this study is to investigate the influences of geometric configuration in coronary artery bypass grafting on the hemodynamic characteristics related to anastomosis.

MATERIALS AND METHODS

1) Geometric shape of the model

The geometric shape of the coronary artery with an aorto-coronary bypass is shown in Fig. 1, and the geometric dimensions of the aorto-cononary bypass models are given in Table 1. The coronary artery is assumed to be a tapered straight vessel with proximal stenosis. The graft angle (θ) is selected as a parameter and is set to be 45°, 60°, or 90°.

The degree of coronary artery stenosis is assumed to be 70% at which point the patient feels chest pain. The geo-

Table 1. Model dimensions of the bypass grafts

Model	d_i	d_0	Remark
Model 1	D_i	D_0	Tapered diameter
Model 2	D_0	D_i	Reversely tapered diameter
Model 3	D_i	D_i	Constant diameter
Model 4	D_0	D_0	Constant diameter

d_i=Inlet diameter of graft vessel; d_0=Outlet diameter of graft vessel; D_i=Inlet diameter of coronary artery; D_0=Outlet diameter of coronary artery. $D_i > D_0$.

metric configuration for the numerical analysis is modeled from the stenosed coronary artery bypassed by a graft vessel with end-to-side anastomosis.

In an aorto-coronary bypass surgery, the autologous conduit is frequently a saphenous vein. Proximal and distal end diameters of the harvested vein graft are usually different.

In order to investigate the influences of the diameter changes of the bypass grafts on hemodynamic characteristics, the proximal and distal end diameters of the graft ($d_i \rightarrow d_0$) were set as shown in Table 1. Di represents the inlet diameter of the stenosed coronary artery and Do represents the outlet diameter which is identical to the the diameter just distal to the end-to-side anastomosis. The diameter of bypass graft in Model 1 is gradually tapered from D_i to D_0 ($D_i > D_0$); and the diameter in Model 2 is reversely tapered from D_0 to D_i, which is the opposite of Model 1. The diameters of the bypass grafts in Model 3 and Model 4 are not changed and uniformly D_i and D_0, respectively.

2) Numerical analysis

(1) Governing and constitutive equations: The following governing equations are used for the numerical analysis. Eqs. (1) and (2) are continuity and momentum equations for 3-dimensional, steady, and incompressible flows.

$$\frac{\partial u_j}{\partial x_j} = 0 \qquad (1)$$

$$p u_j \frac{\partial u_i}{\partial x_j} = -\frac{\partial p}{\partial x_i} + \frac{\partial \tau_{ij}}{\partial x_j} \qquad (2)$$

where p, u_i, and p are the density, velocity vector, and pressure, respectively. The shear stress tensor, τ_{ij}, in Eq. (2) may be expressed as the shear rate in Eq. (3):
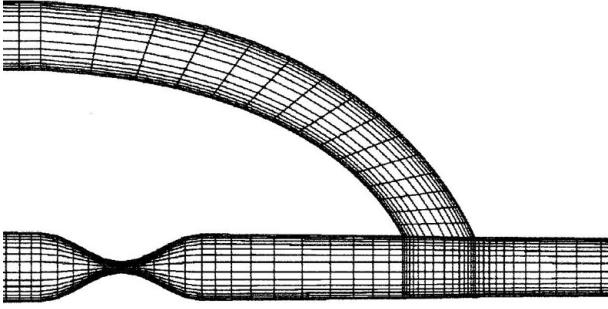
Fig. 2. Geometric mesh of the model for numerical analysis.

$$\tau_{ij} = \eta \left(\frac{\partial u_i}{\partial x_j} + \frac{\partial u_j}{\partial x_i} \right) \qquad (3)$$

where η denotes the apparent viscosity.

Once the local shear rate is calculated, the local non-Newtonian viscosity can be determined from the viscosity model

To take into account the non-Newtonian viscosity effect of blood, a constitutive equation that represents the apparent viscosity of blood as a function of the shear rate is needed. Among various constitutive equations, the Carreau model, well-known rheological simulation model for a non-Newtonian fluid, in Eq. (4) is used to specify the apparent viscosity of blood as a function of shear rate.

$$\eta = \eta_\infty + (\eta_0 - \eta_\infty)[1 + (\lambda\gamma)^2]^{\frac{(q-1)}{2}} \qquad (4)$$

where γ denotes the shear rate. η_∞ and η_o are the apparent viscosities at infinite-shear-rate and zero-shear-rate, respectively. λ and q represent the characteristic time and index of this model, respectively. Rheological values of blood as a non-Newtonian fluid are taken to be η_o=0.056 Pa s, η_∞ =0.00345 Pa s, λ=3.313 s, and q=0.356. Once the local shear rate is calculated, the apparent viscosity of blood can be determined by Eq. (4).

(2) Numerical method: Distributions of velocity and shear stress of blood flow in aorto-coronary artery are obtained by solving the governing equations. The governing equations are discretized with non-staggered grid systems using a finite volume method. In the non-staggered grid system, the velocity components such as u, v, and w in the momentum equations are calculated for the same points that lie on the grid points of pressure. This grid system not only simplifies the discretization equations but also reduces the memory space required for computation efficiently. However, it may bring out the chequerboard oscillation when calculating the pressure field. This oscillating problem is removed by adopting the Rhie-Chow algorithm which is necessary for flow simulations using a collocated grid. The fully implicit scheme is utilized to solve the physiological flow problem, where the time step is set to be 0.01second. The hybrid scheme is adopted for discretizing the convective term and the SIMPLE algorithm for treating the pressure term in the governing momentum equations. A two-dimensional mesh of the aorto-coronary bypass is shown in Fig. 2.

RESULTS

The mass flow rates $\dot{m}_1$, $\dot{m}_2$ and $\dot{m}_0$ represent the rates through the stenosed coronary artery, the bypass graft, and the outlet coronary artery, respectively (Table 2). Rate $\dot{m}_0$ is the sum of $\dot{m}_1$ and $\dot{m}_2$. The mass flow rate is determined by the conservation equations of mass.

Model 3 delivers the largest amount of flow rate among the models studied. This phenomenon is related to the large bypass diameter and the least flow. In the case of the artificial arteries, Model 3 delivers approximately 10% more blood than Model 4. This implies that the larger the bypass diameter, the greater the mass flow rate guaranteed in the anastomosis. In case of the models with tapered or reversely tapered diameter, Model 2 delivers approximately 1% more blood than Model 1 even though the difference between the flow rates of the two models is not significant.

As the anastomotic angle in Model 3 is changed from 45° to 60°, the flow rate of the model is increased by about 4%. This increase is also seen in Model 2 and Model 4. Major flow occurs through the bypass graft and only a minimal amount of blood flows through the stenosed coronary artery (Table 2).

For a given single artery, the pressure drop depends on the mass flow rate through the artery. However, for a given artery system such as the models in this study, the pressure drop along the stenosed coronary artery is related to the mass flow rates through the coronary artery and bypass graft. The

Table 2. Comparison of the mass flow rates for different models

Mass flow rate	Anastomotic angle	Model 1	Model 2	Model 3	Model 4
m_1 (g/s)	45°	0.444	0.399	0.316	0.528
	60°	0.466	0.376	0.304	0.481
	90°	0.362	0.288	0.246	0.388
m_2 (g/s)	45°	3.060	3.140	3.430	2.832
	60°	3.094	3.324	3.600	3.050
	90°	2.714	3.216	3.286	2.584
m_0 (g/s)	45°	3.504	3.539	3.746	3.360
	60°	3.560	3.700	3.904	3.531
	90°	3.077	3.504	3.532	2.971

m_1=Mass flow rate through the stenosed coronary artery; m_2=Mass flow rate through the bypass graft; m_0=Mass flow rate through the outlet coronary artery.
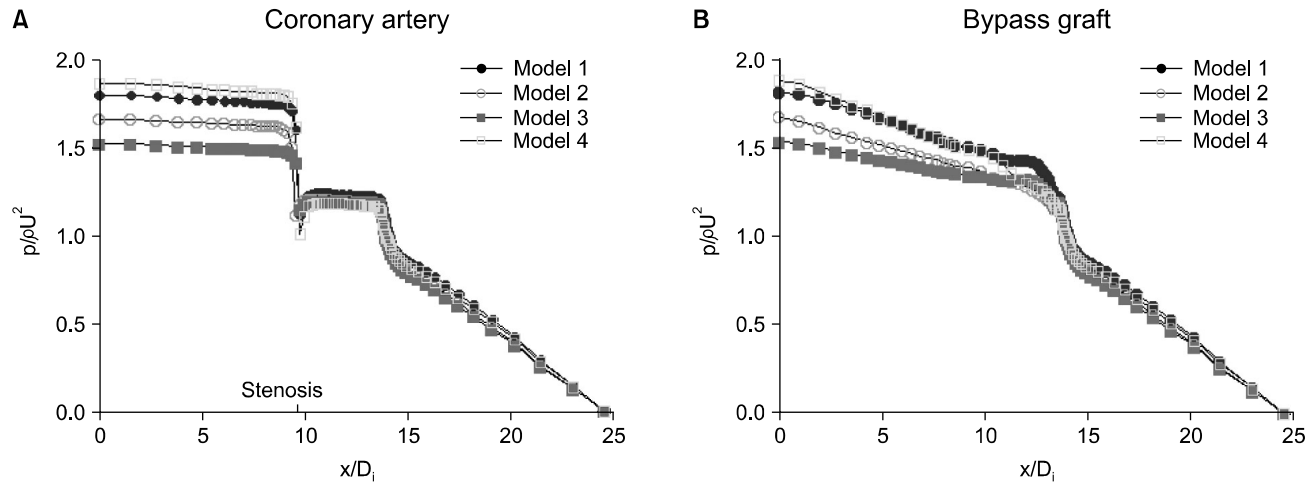

Fig. 3. Pressure variations along the coronary arteries and bypass grafts for an anastomotic angle of 45°.

geometric dimensions and shapes of the coronary and bypass arteries play important roles in the pressure drop characteristics along the arteries. Model 3 delivers the least amount of blood through the stenosed coronary artery because this model has the least flow resistance in the bypass graft. The same reason applies to Model 4, which has the largest flow resistance in the bypass graft. In comparing the mass flow rates, the bypass grafts in Model 3 and 4 are the idealized uniform arteries of different diameters, with Model 3 having a greater diameter and Model 4 a smaller diameter; Model 3 shows much less flow resistance in the bypass graft than Model 4 does.

In order to investigate the effects of the geometric dimensions on the hemodynamic characteristics, the pressure variations along the coronary artery and bypass graft with an angle of 45° are presented in Fig. 3. All the models show a similar tendency toward pressure variation along the coronary artery in Fig. 3A. However, the pressure drop along the coronary artery of each model is different due to the change in the incoming flow rate through the bypass artery.

Models 1 and 2 represents idealized bypass grafts with increasing or decreasing diameters, having orientations opposite each other for the aorto-coronary bypass. Model 1 shows a larger pressure drop than that of Model 2. This implies that the pressure drop along the host coronary artery and the graft is strongly affected by the geometric orientation of the graft in the given anastomotic angle. From Table 2, it can be seen that Model 1 delivers more mass flow through the stenosed
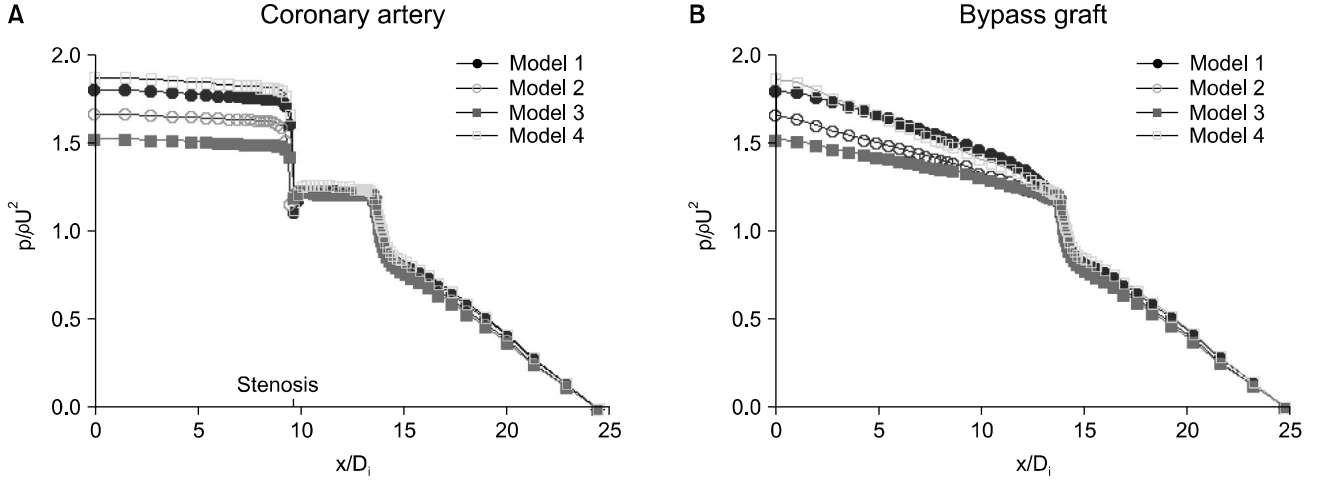
A Coronary artery **B** Bypass graft

Fig. 4. Pressure variations along the coronary arteries and bypass grafts for an anastomotic angle of 60°.

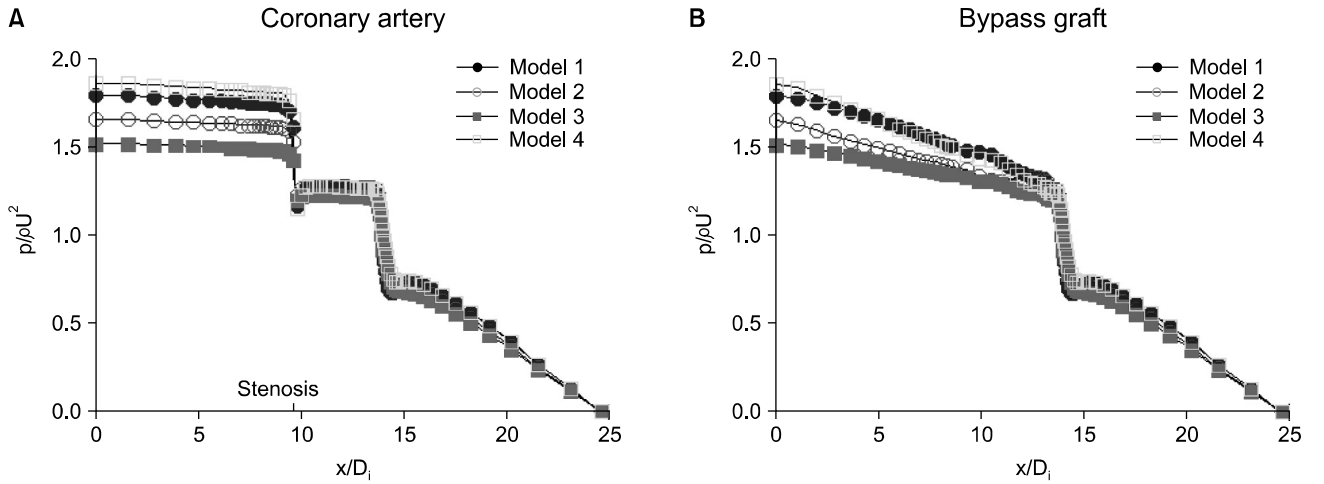**A** Coronary artery **B** Bypass graft

Fig. 5. Pressure variations along the coronary arteries and bypass grafts for an anastomotic angle of 90°.

coronary artery than Model 2. However, Model 2 delivers more mass flow through the bypass artery than Model 1. On the whole, Model 2 delivers more mass flow and experiences a smaller pressure drop than Model 1.

The pressure variations along the bypass arteries are presented in Fig. 3B. The general tendency of the pressure variation along the bypass artery is similar to that of the coronary artery. Model 3 shows the smallest pressure drop, and Model 1 shows the largest pressure drop along the bypass artery. Pressure variations for the anastomosis angles of 60° and 90° are also calculated in this study. No significant differences are found for the different anastomotic angle. Results of the pressure drop along the coronary artery and bypass graft for

the anastomotic angle of 60° and 90° are presented in Fig. 4 and 5.

Distributions of the dimensionless wall shear stress are shown in Fig. 6 to investigate the effects of the anastomotic angle. Wall shear stress distributions along the outer wall of the bypass graft for the anastomotic angles of 45°, 60° and 90° are presented in Fig. 6, respectively. For the given anastomotic angle and model, the wall shear stress in the proximal region of the bypass graft is almost constant except for the area very close to the toe site. The wall shear stress value is slightly different depending on the models. The wall shear stress values vary slightly depending on the shape of the artery. A slight increase in wall shear stress in Model 1 and
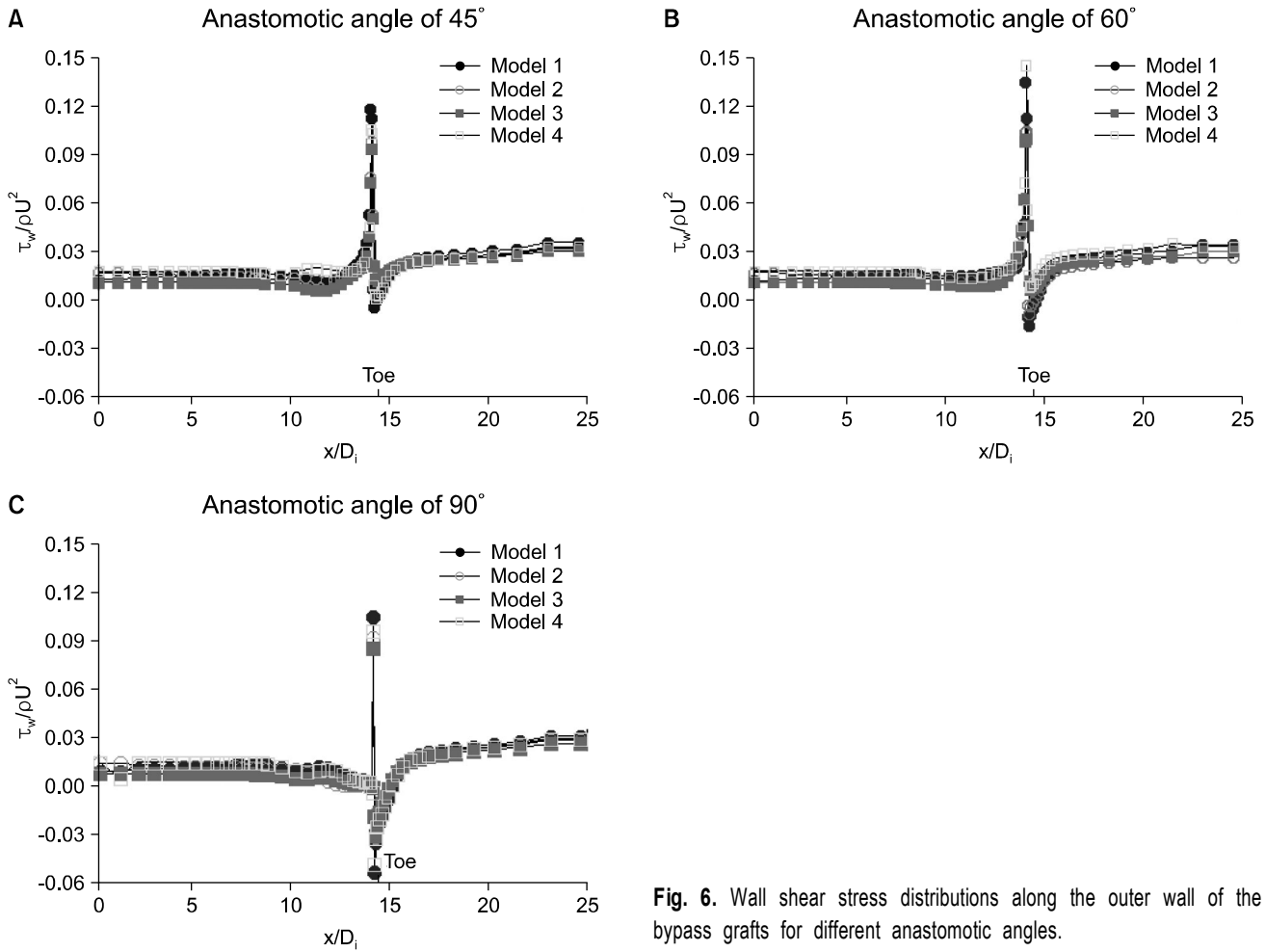
A Anastomotic angle of 45°

B Anastomotic angle of 60°

C Anastomotic angle of 90°

Fig. 6. Wall shear stress distributions along the outer wall of the bypass grafts for different anastomotic angles.

slight decrease in Model 2 along the upstream artery of the proximal region are observed in this figure.

The wall shear stresses of all models increase rapidly as the flow approaches the toe site, showing their maximum values at the toe. Shear stress decreases sharply just downstream of the toe site, showing its minimum negative value. The shear stress increases rapidly just downstream of the toe and reaches its developed value as the flow moves far downstream. The negative value of the wall shear stress in the distal region just downstream of the toe implies that the flow reversal phenomenon prevails in that region. The wall shear stress along the bypass is larger than that along the outer wall of the stenosed coronary artery.

In the upstream region of the toe, the wall shear stress values of all models for the anastomotic angle of $45°$ are larger than those for the angle of $60°$. However at the site near the

toe, the maximum values of the wall shear stress for the angle of $60°$ are larger than those for the angle of $45°$. The wall shear stress distributions along the outer wall of the stenosed coronary artery are shown in Fig. 7. The wall shear stresses of all the models are very similar and small because the flow rates through the stenosed coronary artery of all the models are much smaller than those through the bypass grafts.

The wall shear stress distributions along the inner wall of the bypass grafts for the different anastomotic angles are shown in Fig. 8. The shear stresses vary slightly depending on the model, but the differences are negligible in the upstream region of the heel. However, the anastomotic angle effect is quite significant near and at the heel site. The shear stress near the heel site increases rapidly at the anastomotic angle of $60°$.
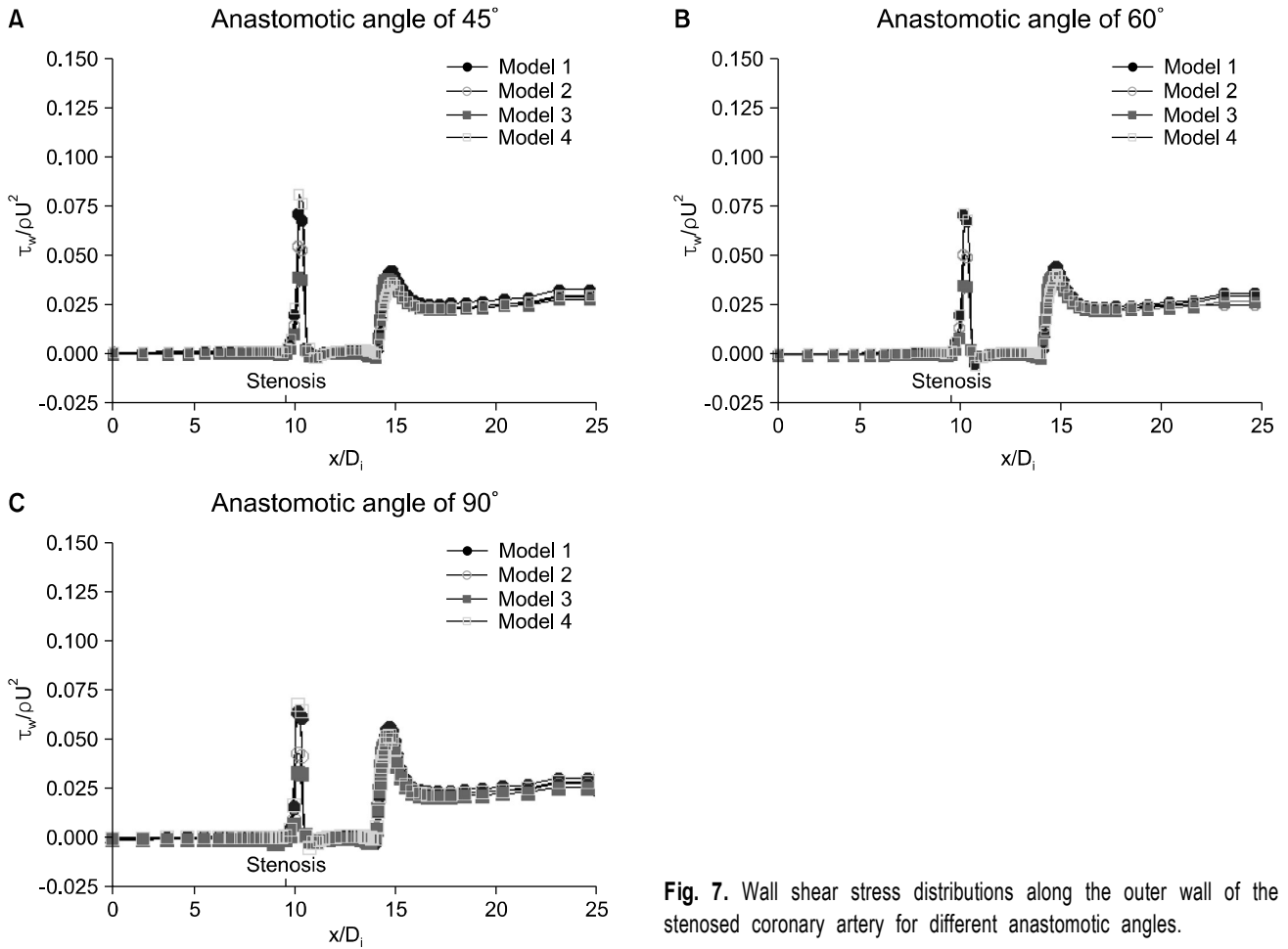
Fig. 7. Wall shear stress distributions along the outer wall of the stenosed coronary artery for different anastomotic angles.

DISCUSSION

This study showed the effects of the geometric dimension (bypass graft diameter and tapered direction) and the anastomotic angle on the mass flow rate, pressure drop, and wall shear stress along the stenosed coronary artery and end-to-side bypass graft by using numerical simulation. These effects are summarized as follows:

(1) Model 3 delivers the largest amount of mass flow and the least pressure drop along the bypass graft. It is recommended that a uniform bypass graft whose diameter is the same as the inlet diameter of the stenosed coronary artery be used.

(2) Orientation of the nonuniform bypass graft is an important biomechanical factor. When comparing the two non-uniform graft models, Model 2, where the inlet diameter is smaller than the distal diameter, is preferable to Model 1, where the inlet diameter is larger and tapered off.

(3) Formation of the recirculation zones along the outer walls at the region distal to the anastomosis depends on the geometric shape of the bypass graft and the anastomotic angle.

(4) The wall shear stresses of all models near the toe and heel are strongly affected by the geometric shape of the by-pass graft and the anastomotic angle. The wall shear stress along the outer wall of the bypass graft increases abruptly near the toe for all models and all anastomotic angles. Near the heel, however, the rapid increase of wall shear stress along the inner wall of the bypass graft can only be seen at the anastomotic angle of $60°$.

Although the use of an arterial graft may improve long-term graft patency, a saphenous vein graft is still widely

A Anastomotic angle of 45°

B Anastomotic angle of 60°
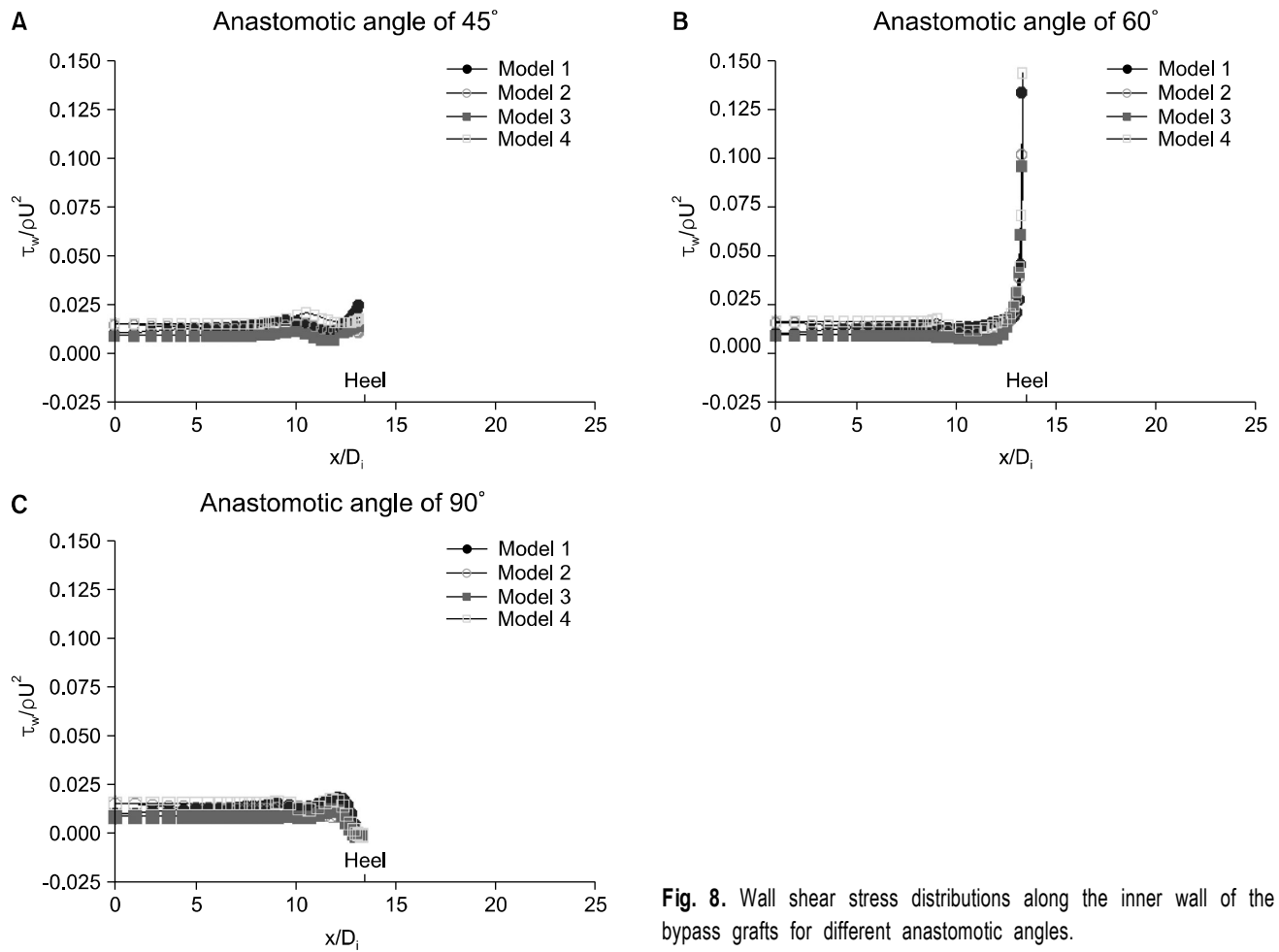

C Anastomotic angle of 90°

Fig. 8. Wall shear stress distributions along the inner wall of the bypass grafts for different anastomotic angles.

used for aorto-coronary bypass. Numerical studies on the etiology of perianastomotic neointimal hyperplasia, which sets the foundation of the later atherosclerotic process [15,16], have been performed in order to improve graft patency, in particular, of the saphenous vein graft. However, relatively little is known about any biomechanical factors which may play an important etiologic role. This study based on computational and mathematical models demonstrated part of the relevant biomechanics of the bypass grafts, which should be further elucidated. In terms of anastomotic neointimal hyperplasia, several hypotheses have been suggested including a compliance mismatch between the graft and host artery [17], high frequency flow and wall shear stress [18], and abnormal flow dynamics at the distal anastomosis [19].

According to a recent review [9], the relevant biomechanical factors predisposing to host coronary artery and bypass graft disease are classified into primary and secondary factors. The primary biomechanical factors are (1) low-wall shear stress or highly oscillatory wall shear stress and (2) high-wall mechanical stress or strain. The secondary biomechanical factors include vessel wall characteristics and the presence of reflection waves, vessel geometry, and vessel movement. Low-wall shear stress is associated with plaque thickening [20] and increased atherosclerosis progression [21] for several possible reasons: unfavorable alignment with the flow direction and shape of the endothelial cells [22]; increased uptake of atherogenic particles [23]; or decreased oxygen flux into the vessel wall [24]. High-wall stress, resulting in localized stress concentration and pressure distension of the bypass graft, is associated with being susceptible to atherosclerosis [25]. Several possible reasons for this have been proposed: generation of reactive oxygen species and up-

regulation of redox-sensitive pro-inflammatory gene products stimulated by mechanical arterial wall deformation [26]; expression of endothelial adhesion molecules resulting from pressure distension of the saphenous vein [27]; or proliferation of the smooth muscle cells stimulated by pulsatile stretch [28]. The results of this study indicated effects of the geometric dimensions and the bypass angle of the graft as possible secondary biochemical factors that could directly affect the primary biomechanical factors.

This study showed that severe variation of the wall shear stress occurs at the toe and heel sites and that the anastomotic angle plays a very important role in wall shear stress and the shear stress gradient. High wall shear stress and the shear stress gradient near and at the toe and heel may result in altered fluid dynamics as demonstrated by Freshwater et al. [29] with computational models.

Generally, the wall shear stress is lowest along the inner curvature and it becomes greater as the curvature increases [9]. This is partly in line with the results of this study. At the anastomotic angle of 45° and 90°, the wall shear stress along the inner curvature of the bypass graft and at the heel were small. However, at the angle of 60°, the wall shear stress increased rapidly near the heel, which is interesting. This observation will be quite valuable knowledge for choosing anastomosis techniques if it is firmly supported by in-vivo studies in the future, considering that the low-wall shear stress and recirculation zone are likely to occur around the heel and are associated with progression of intimal hyperplasia affecting the long-term patency of the bypass graft [29].

CONCLUSION

The present study may have clinical implications and provide insight into the biomechanics of various configurations of end-to-side coronary artery bypass grafting. Although the present study is not based on in-vivo measurement but on the mathematical and computational modeling, these methods are good tools for analyzing the biomechanical factors which are speculated to contribute to graft patency in coronary artery bypass grafting.

REFERENCES

1. Bassiouny HS, White S, Glagov S, Choi E, Giddens DP, Zarins CK. *Anastomotic intimal hyperplasia: mechanical injury or flow induced?* J Vasc Surg 1992;15:708-17.

2. Hofer M, Rappitsch G, Perktold K, Trubel W, Schima H. *Numerical study of wall mechanics and fluid dynamics in end-to-side anastomosis and correlation to intimal hyperplasia.* J Biomech 1996;29:1297-308.

3. Ballyk PD, Walsh C, Butany J, Ojha M. *Compliance mismatch may promote graft-artery intimal hyperplasia by altering suture-line stresses.* J Biomech 1998;31:229-37.

4. Leuprecht A, Perktold K, Prosi M, Berk T, Trubel W, Schima H. *Numerical study of hemodynamics and wall mechanics in distal end-to-side anastomoses of bypass grafts.* J Biomech 2002;35:225-36.

5. Nerem RM. *Vascular fluid mechanics, the arterial wall and atherosclerosis.* J Biomech Eng 1992;114:274-82.

6. Texon M, Imparato AM, Helpern M. *Role of vascular dynamics in the development of atherosclerosis.* JAMA 1965;194:168-72.

7. Fry DL. *Response of the arterial wall to certain physical factors in atherogenesis: initiating factors.* Ciba Found Symp 1973;12:187-204.

8. Caro CG, Nerem RM. *Transport of C-40-cholesterol between serum and wall in the perfused dog common carotid artery.* Circ Res 1973;24:187-204.

9. John LC. *Biomechanics of coronary artery and bypass graft disease: potential new approaches.* Ann Thorac Surg 2009;87:331-8.

10. Friedman MH, Brinkman AM, Qin JJ, Seed WA. *Relation between coronary artery geometry and the distribution of early sudophilic lesions.* Atherosclerosis 1993;98:193-9.

11. Friedman MH, Baker PB, Ding Z, Kuban BD. *Relationship between the geometry and quantitative morphology of the left anterior descending artery.* Atherosclerosis 1996;125:183-92.

12. Friedman MH, Ding Z. *Relation between the structural asymmetry of coronary branch vessels and the angle at their origin.* J Biomech 1998;31:273-8.

13. Inzoli F, Migliavacca F, Pennati G. *Numerical analysis of steady flow in aorto-coronary bypass 3-D model.* J Biomech Eng 1996;118:172-9.

14. Henry FS, Collins MW, Hughes PE, How TV. *Numerical investigation of steady flow in proximal and distal end-to-side anastomosis.* J Biomech Eng 1996;118:302-10.

15. Motwani JG, Topol EJ. *Aortocoronary saphenous vein graft disease: pathogenesis, predisposition, and prevention.* Circulatioin 1998;97:916-31.

16. Dilley RJ, McGeachie JK, Tennant M. *Vein to artery grafts: a morphological and histochemical study of the histogenesis of intimal hyperplasia.* Aust N Z J surg 1992;62:297-303.

17. Abbott WM, Megerman J. *Does compliance mismatch alone cause neointimal hyperplasia?* J Vasc Surg 1989;9:507.

18. Imparato AM, Bracco A, Kim GE, Zeff R. *Intimal and neointimal fibrous proliferation causing failure of arterial reconstructions.* Surgery 1972;72:1007-17.

19. Faulkner SL, Fisher RD, Conkle DM, Page DL, Bender HW Jr. *Effect of blood flow rate on subendothelial proliferation in venous autografts used as arterial substitutes.* Circulation 1975;52:1163-72.

20. Krams R, Wentzel JJ, Oomen JAF, et al. *Evaluation of endothelial shear stress and 3D geometry as factors determining the development of atherosclerosis and remodeling in human coronary arteries in vivo.* Arterioscler ThrombVasc Biol 1997;17:2061-5.

21. Gibson CM, Diaz L, Kandarpa K. *Relation of vessel wall shear stress to atherosclerosis progression in human coronary arteries.* Arterioscler Thromb 1993;13:310-5.

22. Levesque MJ, Liepsch D, Moravec S, Nerem RM. *Correlation of endothelial cell shape and wall shear stress in a stenosed dog aorta.* Arteriosclerosis 1986;6:220-9.

23. Glagov S, Zarins C, Giddens DP, Ku DN. *Hemodynamics and atherosclerosis. Insights and perspectives gained from studies of human arteries.* Arch Pathol Lab Med 1988;112: 1018-31.

24. Perktold K, Leuprecht A, Prosi M, et al. *Fluid dynamics, wall mechanics, and oxygen transfer in peripheral bypass anastomoses.* Ann Biomed Eng 2002;30:447-60.

25. Salzar RS, Thubrikar MJ, Eppink RT. *Pressure-induced mechanical stress in the carotid artery bifurcation: a possible correlation to atherosclerosis.* J Biomech 1995;28:1333-40.

26. Taylor WR. *Mechanical deformation of the arterial wall in hypertension: a mechanism for vascular pathology.* Am J Med Sci 1998;316:156-61.

27. Chello M, Mastroroberto P, Frati G, et al. *Pressure distension stimulates the expression of endothelial adhesion molecules in the human saphenous vein graft.* Ann Thorac Surg 2003;76:453-8.

28. Predel HG, Yang Z, von Segesser L, Turina M, Bühler FH, Lüscher TF. *Implication of pulsatile stretch on growth of saphenous vein and mammary artery smooth muscle.* Lancet 1992;340:878-9.

29. Freshwater IJ, Morsi YS, Lai T. *The effect of angle on wall shear stresses in a LIMA to LAD anastomosis: numerical modelling of pulsatile flow.* Proc Inst Mech Eng 2006;220: 743-57.